

Individual and Multi Vortex Pinning in Systems with Periodic Pinning Arrays

C. Reichhardt

CNLS and Applied Theoretical and Computational Physics Division, Los Alamos National Laboratory, Los Alamos, NM 87545

G.T. Zimányi, R.T. Scalettar

Department of Physics, University of California, Davis, California 95616.

A. Hoffmann

Los Alamos National Laboratory, Los Alamos, NM 87545

Ivan K. Schuller

University of California-San Diego, Department of Physics 0319, La Jolla, California 92093-0319

(October 28, 2018)

We examine multi and individual vortex pinning in thin superconductors with periodic pinning arrays. For multi-vortex pinning we observe peaks in the critical current of equal magnitude at every matching field, while for individual vortex pinning we observe a sharp drop in the critical current after the first matching field in agreement with experiments. We examine the scaling of the critical current at commensurate and incommensurate fields for varied pinning strength and show that the depinning force at the incommensurate fields decreases faster than at the commensurate fields.

PACS numbers: 74.60.Ge, 74.60.Jg

Vortex matter in superconductors with periodic pinning arrays has been studied for several years now starting with the pioneering work of Fiory *et al.* [1]. Recently considerable renewed interest in this system has come about due to advancements in nano-lithographic techniques in which arrays of holes [2–6], defects [7] or magnetic dots [8–13] can be created where various parameters such as the pinning strength, size, and periodicity can be carefully controlled. These experiments have observed interesting commensurability effects where the critical current shows a maximum and magnetoresistance a minimum when the number of vortices equals an integer multiple of the number of pinning sites. In addition peaks in the critical current have also been observed at some fractional matching fields [3]. Many applications of superconductors require high critical currents and the nano-engineered periodic pinning systems may be able to provide optimal pinning. A key question that needs to be understood in order for optimal pinning arrays to be constructed is where and how the vortices are arranged at the varied matching fields. In particular, it is not clear whether there are multiple vortices located at individual pinning sites above the first matching field or whether only one vortex sits at an individual pinning site, nor has it been shown how this ordering affects the observed commensuration effects.

In magnetization experiments in anti-dot lattices [2] it was observed that the critical current dropped abruptly beyond a specific matching field which depends on temperature. It was inferred that below this field the pinning sites were capturing multiple vortices that could be

strongly pinned, and that beyond this field the additional vortices were located in the interstitial regions and were not pinned directly by the pinning sites. On the other hand imaging experiments using Lorentz microscopy [7] of vortices in periodic pinning arrays observed only one vortex being trapped per pinning site and showed that at the integer matching fields the vortices form highly ordered crystals with the crystal symmetry depending on the particular matching field. Subsequent simulations of vortices in periodic pinning arrays where only one vortex can be trapped at a pinning site also produced the same types of vortex crystals observed in the Lorenz microscopy experiments at the matching fields [14]. In addition the simulations also showed that peaks in the critical current occur at those matching fields where the interstitial vortices can form a highly ordered structure; however, some matching fields did not show a peak in the critical current, and the magnitude of the commensuration effect varied considerably at different matching fields. Recent experiments with small pinning sites where it is expected that only one vortex can be pinned at an individual pinning sites observed commensuration peaks in agreement with these simulations [4]. There is also evidence from decoration experiments [5] that multi-vortex pinning at individual pinning sites in periodic pinning arrays occurs. Other recent imaging experiments with Hall probe arrays have also observed multi-vortices at individual pinning sites and show that above a certain field, additional vortices sit in the interstitial regions [6]. These experiments seem to indicate that when multi-vortex pinning occurs the vortices in the pinning site merge to form

a macro-vortex.

Another open question in vortex pinning in periodic arrays is why the commensuration effects are only pronounced near T_c . One proposal is that the bulk pinning increases at low T and washes out the effect of the periodic pins; however, samples with periodic pinning always show a much higher critical current than comparison samples without the periodic pinning even for low T , indicating that the periodic pinning is still effective at low T .

In this work we present results from simulations to elucidate the response of the critical current with multi-vortex vs individual vortex pinning. We model the multi-vortices as individual vortices with increased number of flux quanta. We find that with multi vortex pinning, peaks in the critical current of the same magnitude occur at every matching field. For individual vortex pinning the critical current drops off after the first matching field. These results agree well with experimental results for vortices interacting with magnetic dots where with large dots multi-vortex pinning could be expected. We also examine the scaling of the depinning force at commensurate and incommensurate fields as a function of the pinning strength. For all pinning strengths examined we find that depinning force scales linearly with pinning strength at commensurate fields. For incommensurate fields the depinning force scales linearly for large pinning forces but shows a crossover to a faster than linear scaling with smaller pinning strengths. This result may explain why commensurability effects are most pronounced for high temperatures where the pinning is reduced. In addition we also examine the scaling of the critical current at the second matching field for multi-vortex pinning and individual pinning and find that as the pinning strength is increased the critical current saturates when individual vortex pinning is present.

We model vortices in a 2D superconductor interacting with a square pinning array. The overdamped equation of motion for a vortex i is

$$\mathbf{f}_i = \frac{d\mathbf{r}_i}{dt} = \mathbf{f}_i^{vv} + \mathbf{f}_i^{vp} + \mathbf{f}_d = \eta \mathbf{v}_i \quad (1)$$

Here, \mathbf{f}_i^v is the force from the other vortices, \mathbf{f}_i^{vp} is the force from the pinning, \mathbf{f}_d is the applied driving force corresponding to a Lorentz force from an applied current, and η is the damping which we set to unity. We model the vortex-vortex interaction potential as $U_v = \ln(r)$ which is appropriate for thin film superconductors. We have also conducted simulations using the modified Bessel function interaction potential $K_0(r)$ which is appropriate for bulk superconductors. The total force on vortex i from the other vortices is $\sum_{j \neq i}^{N_v} \nabla_i U_v(r_{ij})$. We impose periodic boundary conditions in the x and y directions. For the long-range logarithmic interaction we use an exact and fast converging sum [15]. The pinning is modeled as attractive parabolic wells of radius r_p .

$$f_i^{vp} = (f_p/r_p)(\mathbf{r}_i - \mathbf{r}_k^p)\Theta(|\mathbf{r}_i - \mathbf{r}_k^p|/\lambda). \quad (2)$$

Here, Θ is the Heaviside step function, $\mathbf{r}_k^{(p)}$ is the location of pinning site k , f_p is the maximum pinning force, and λ is the penetration depth. The pinning is placed in a square array. The initial vortex positions are obtained from annealing from a high temperature where the vortices are in a molten state and gradually cooling to $T = 0$. After the vortex configurations are obtained the critical depinning force is determined by applying a slowly increasing uniform force. We simulate two models. In the first, the pinning sites are small and can capture only one vortex each, so for fields greater than the first matching field additional vortices are located between the pinning sites. In the second model, multiple vortices can be captured by larger pinning sites, and we assume that the vortices in the pinning sites coalesce and form a single multiple-quantized vortex. The multi-vortices interact with other vortices as $n\ln(r)$ where n is the quantization of the vortex. Beyond the first matching field we start the simulation by annealing with the number of multiple quantized vortices already fixed so that we do not actually model the merging of the vortices. The multi-quantized vortices will still feel the same pinning force as the individual vortices. This is a reasonable assumption if the core of the vortex is smaller than the pinning site, since the maximum pinning force is determined by the gradient of the potential energy of the pinning site, which should not be affected by the size of the vortex.

In Fig. 1 we show the critical depinning force f_p^c versus field for the case where multiple vortex pinning occurs (thick curve) and for the case of single vortex pinning (thin curve). For $B/B_\phi < 1.0$ the depinning force is the same for both pinning radii which is due to the fact that the maximum pinning force for the pinning sites are the same. A peak at $B/B_\phi = 1/2$ occurs which is due to the formation of an ordered state as seen in previous simulations and experiments. There is a peak in both curves at the the first matching field where the vortex lattice has the same symmetry as the pinning lattice. For fields greater than $B/B_\phi = 1.0$ the curves deviate, with the single vortex pinning curve dropping substantially while the multiple vortex pinning curve only decreases by a small amount. The height of the peak for the multi-vortex curve at $B/B_\phi = 2.0$ and the higher matching fields is the same as that for $B/B_\phi = 1.0$ since in our model the multiple vortices experience the same pinning force as the singly quantized vortices. The multi-vortex curve also shows matching peaks at the fractional fields $n/2$. For the single vortex pinning curve the maximum critical depinning force at $B/B_\phi = 2.0$ is much lower than that for the multi-vortex case. The fractional matching peaks are also suppressed for the individual vortex pinning case.

The vortex configurations where only one vortex is captured per pinning site are the same as those observed in

previous experiments and simulations. The vortex configurations for the multi-vortex pinning case repeat for each matching field with a square overall vortex lattice at each matching field composed of multiply quantized vortices.

In Fig. 2 we show the results of transport experiments for Nb films with square periodic arrays of magnetic Ni dots for two different sized dots. Here the period is $a = 600\text{nm}$ and the upper curve has a dot diameter of $d = 400 - \text{nm}$ and the lower curve $d = 530 - \text{nm}$ and $T = 0.98T_c$. Additional information about the fabrication of the arrays can be found in Ref[8]. The values of $\rho(H)$ for both sized dots is roughly the same for $B/B_\phi = 1.0$ with the ρ minima values at $B/B_\phi = 1.0$ being the same. For $B/B_\phi > 1.0$ the $d = 400 - \text{nm}$ pinning is greatly reduced as seen by the increase in $\rho(H)$; however, minima still occur at the higher matching fields. In contrast the ρ values for the $d = 530 - \text{nm}$ show only a minimal increase with H and pronounced matching minima of approximately the same magnitude at each field are observed. This result agrees well with the simulations, suggesting that for the larger dots, multi-vortex pinning is occurring at each matching field, while for the smaller dots, only one vortex is being trapped at each dot and additional vortices are located in the interstitial regions.

In Fig. 3 we show that commensurability effects become more pronounced for weaker pinning. We consider multi-vortex pinning for $f_p = 0.8$ and 0.1 . Fig. 3 shows f_p^c/f_p for the two pinning strengths. At the matching fields the depinning force equals the pinning force. At the incommensurate fields the relative depinning force is much lower for the weaker pinning sample.

In order to quantify the behavior observed in Fig. 3, in Fig. 4(a) we examine the depinning force for the commensurate field $B/B_\phi = 1.0$ and the incommensurate field $B/B_\phi = 0.64$ for a series of simulations with varied f_p . The depinning force for $B/B_\phi = 1.0$ decreases linearly with $f_p^c \propto f_p$ which is the individual pinning regime. Since the vortex lattice is perfectly symmetric at the matching field, the vortex-vortex interactions cancel so the depinning force is determined only by the pinning energy. For $B/B_\phi = 0.64$, where vortex-vortex interactions should be relevant, we observed that for large f_p the depinning force again decreases linearly with f_p ; however, near $f_p = 0.2$ there is a crossover to faster than linear decrease with $f_p^c \propto f_p^{1.42}$. We have found the same behavior for other incommensurate fields; thus, the difference in the critical current between the commensurate and the incommensurate fields grows as f_p is lowered. This behavior could account for the pronounced matching peaks only near T_c where the pinning is weak. We were not able to go to weaker pinning where one might expect a crossover to a collective pinning regime with $f_p^c \propto f_p^2$.

To compare the effect of pinning strength on the criti-

cal current for individual versus multiple vortex pinning we have conducted a series of simulations at $B/B_\phi = 2.0$ for varied f_p for the two cases. In Fig. 4(b) we show that f_p^c for the multi-vortex pinning case increases linearly with f_p . We have also found the same linear increase at the other matching fields for the multi-vortex pinning case. The depinning in the multi-vortex case occurs in one stage with the entire lattice depinning at once. For the individual vortex pinning case there is an initial increase in f_p^c for low values of f_p followed by a saturation. This saturation can be understood by considering that the pinning of the interstitial vortices is caused by the repulsion of the vortices at the pinning sites which is independent of the pinning strength. The saturation point also marks the onset of a two stage depinning process where the interstitial vortices depin first followed by the vortices at the pinning sites at a higher drive. A two stage depinning transition at $B/B_\phi = 2.0$ has been observed in experiments for widely spaced hole arrays [16]. Below the saturation point the entire lattice depins simultaneously.

In conclusion we have compared multiple and individual vortex pinning in periodic pinning arrays. We find that with multiple vortex pinning, peaks in the critical depinning force occur at every matching field with the same amplitude. For individual vortex pinning the depinning force drops markedly for $B/B_\phi > 1.0$; however, peaks at the matching field are still present. These results are in good agreement with transport measurements on periodic magnetic dot arrays for different dot sizes with the smaller dot systems showing results consistent with individual pinning while the larger dot systems show results constant with multiple vortex pinning. We also show that the commensurability effects are more pronounced for weak pinning, with the critical depinning force decreasing linearly with decreasing pinning force while the depinning force at incommensurate fields decreases faster than linear. For multi-vortex pinning the critical depinning force scales linearly with pinning force at all matching fields while for individual pinning there is a saturation effect of the critical depinning force.

Acknowledgments We thank C.J. Olson for critical reading of this manuscript, and S. Bending, S. Field, and V. Metlushko for useful discussions. This work was supported by NSF-DMR-9985978, CLC and CULAR (Los Alamos National Laboratory).

[1] A.T. Fiory, A.F. Hebard, and S. Somekh, *Appl. Phys. Lett.* **32**, 73 (1978).
[2] M. Baert *et al.*, *Phys. Rev. Lett.* **74**, 3269 (1995).
[3] M. Baert *et al.*, *Europhys. Lett.* **29**, 157 (1995);
V.V. Moshchalkov *et al.*, *Phys. Rev. B* **54**, 7385 (1996);

V.V. Moshchalkov *et al.*, Phys. Rev. B **57**, 3615 (1998); V.V. Metlushko *et al.*, Phys. Rev. B **59**, 603 (1999).

[4] V.V. Metlushko *et al.*, Phys. Rev. B **60**, R12 585 (1999).

[5] A. Bezryadin and B. Pannetier, J. Low Temp. Phys. **102**, 73 (1996).

[6] A.N. Grigorenko *et al.*, Phys. Rev. B **63**, 05204 (2001); S. Field *et al.*, cond-mat/0003415.

[7] K. Harada *et al.*, Science **271**, 1393 (1996).

[8] J.I. Martín *et al.*, Phys. Rev. Lett. **79**, 1929 (1997); Y. Jaccard *et al.*, Phys. Rev. B **58**, 8232 (1998); A. Hoffmann, P. Prieto and I.K. Schuller, Phys. Rev. B **61**, 6986 (2000).

[9] J.I. Martín *et al.*, Phys. Rev. Lett. **83**, 1022 (1999); J.I. Martín *et al.*, Phys. Rev. B **62**, 9110 (2000).

[10] M.J. Van Bael, Phys. Rev. B **59**, 14674 (1999); M. Lange *et al.*, cond-mat/0012428.

[11] Y. Fasano *et al.*, Phys. Rev. B **60**, R15047 (1999).

[12] D.J. Morgan and J.B. Ketterson, Phys. Rev. Lett. **80**, 3614 (1998).

[13] A. Terentiev *et al.*, Physica C **324**, 1 (1999); A. Terentiev *et al.*, Phys. Rev. B **61**, R9249 (2000).

[14] C Reichhardt, C.J. Olson, and F. Nori, Phys. Rev. B **57**, 7937 (1998).

[15] N. Grønbech-Jensen, Int. J. Mod. Phys. C **57**, 2574 (1998); N. Grønbech-Jensen, Comp. Phys. Comm. **119**, 115 (1999).

[16] E. Rossel *et al.*, Phys. Rev. B **53**, 2983 (1996).

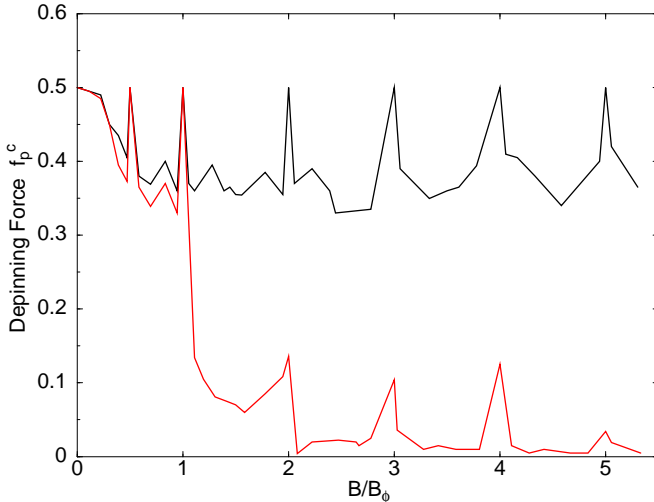


FIG. 1. Critical depinning force as a function of vortex density for samples with square arrays of pinning sites. The upper curve (thick lines) is the depinning system with multiple vortex pinning for $B/B_\phi > 1.0$, $r_p = 0.5$ and lower curve is the depinning line for a system when only one vortex is captured at a pinning site.

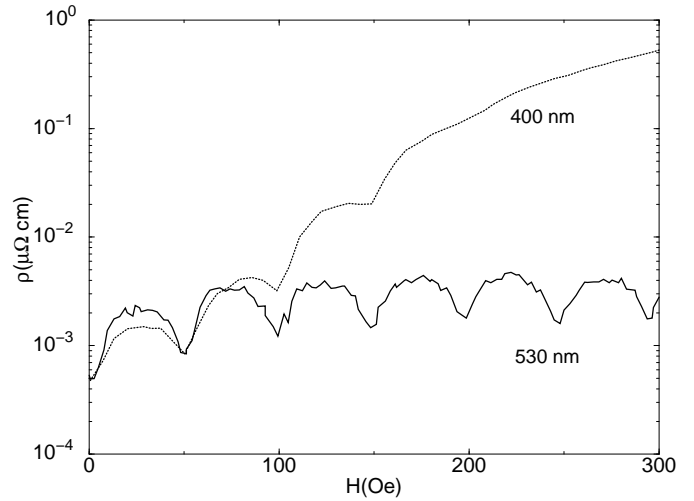


FIG. 2. Experimental values of $\rho(H)$ for Nb samples with square arrays of Ni dots for two different dot diameters 530 nm (solid line) and 400 nm (dashed line) at $T/T_c = 0.98$.

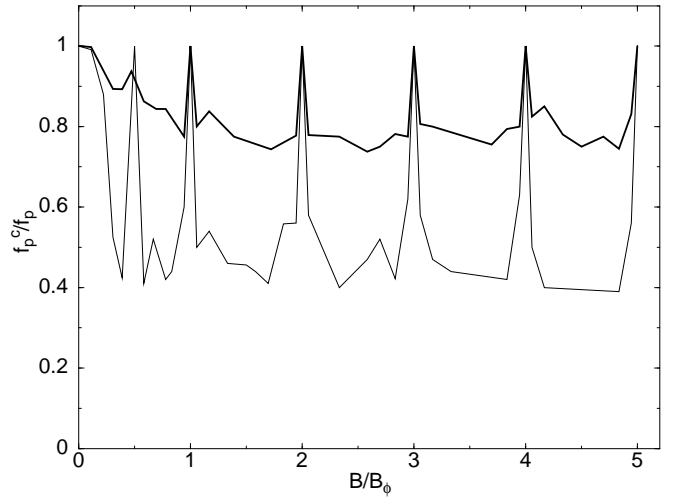


FIG. 3. The normalized depinning force vs B/B_ϕ for $f_p = 0.8$ upper curve (thick lines) and $f_p = 0.1$ lower curve (thin line) obtained from simulations. Multi-vortex pinning occurs for $B/B_\phi > 1.0$. Here the commensurability effects can be seen to be more pronounced for the weaker pinning sample.

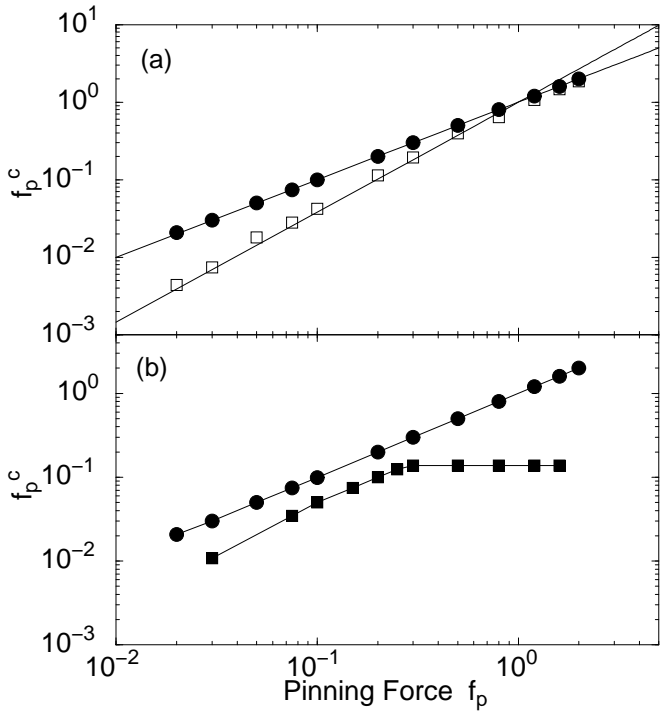


FIG. 4. (a) The depinning force vs f_p for $B/B_\phi = 1.0$ (filled circles) and $B/B_\phi = 0.64$ (open circles). The depinning force for B/B_ϕ goes linearly with f_p as shown with the fit while the depinning force for $B/B_\phi = 0.64$ goes as $f_p^{1.42}$ as shown with the fit. For $f_p > 1.0$ the depinning force for $B/B_\phi = 0.64$ crosses over to a linear behavior. (b) The depinning force for $B/B_\phi = 2.0$ for multi-vortex pinning (filled circles) and for single vortex pinning (filled squares). For the single vortex pinning there is a saturation in the depinning force for $f_p > 0.3$ while the multi-vortex pinning case increases linearly with f_p .